Konstantin Rozov*, Hilde Curtius, and Dirk Bosbach

Preparation, characterization and thermodynamic properties of Zr-containing Cl-bearing layered double hydroxides (LDHs)

Abstract: Zr-containing layered double hydroxides (LDHs) with variable $x\mathrm{Zr}_{\mathrm{solid}} = \mathrm{Zr}/(\mathrm{Zr} + \mathrm{Al})$ mole fractions were synthesized by a co-precipitation method at ambient conditions. The chemical compositions of samples and corresponding aqueous solutions after syntheses were analyzed by ICP-OES, EDX (Mg, Al, Zr) and ion chromatography (Cl^-). Results of PXRD technique demonstrated that solids with $0 \le x\mathrm{Zr}_{\mathrm{solid}} \le 0.5$ show only X-ray reflexes typical for pure LDH compositions, while products of syntheses with $x\mathrm{Zr}_{\mathrm{solid}} > 0.5$ display additional patterns attributed to brucite. ICP-OES and EDX techniques shown that in pure Zr-containing LDHs the Mg/(Al + Zr) ratio is reducing with increase of $x\mathrm{Zr}_{\mathrm{solid}}$ and the stoichiometry of brucite-like layers corresponds to $[\mathrm{Mg}_{3-2x}\mathrm{Al}_{1-x}\mathrm{Zr}_x]$. This fact may indicate that the incorporation of 1 Zr-containing specie results in the removal of 1 Al- and 2 Mg-containing species from the pure Mg-Al-composition. Such mechanism may be confirmed by the observation that measured $a_0 = b_0$ distances are generally consistent with theoretical estimates obtained from $[\mathrm{Mg}_{3-2x}\mathrm{Al}_{1-x}\mathrm{Zr}_x]$-stoichiometry. The presence of predominant Mg^{2+}, $Al(OH)_4^-$ and $Zr(OH)_5^-$ complexes in aqueous solutions after syntheses was established in thermodynamic calculations by applying GEMS-Selektor v.3. code and, therefore, the reaction: $\mathrm{Mg_3Al_1(OH)_8Cl_1} + \mathrm{Zr(OH)_5^-} = \mathrm{Mg_1Zr_1(OH)_5Cl_1} + \mathrm{Al(OH)_4^-} + 2\,\mathrm{Mg^{2+}} + 4\,\mathrm{OH^-}$ can describe a mechanism of Zr-substitution. Estimates of the molar Gibbs free energies of Zr-containing LDHs with $0 \le x\mathrm{Zr}_{\mathrm{solid}} \le 0.5$ show that the incorporation of Zr into the LDH increasing significantly their aqueous solubility. Thus, it is not possible to neglect that Zr can be partly localized as $Zr(OH)_5^-$-ligands in the interlayer space of the LDH structure.

***Corresponding author: Konstantin Rozov,** Institute of Energy and Climate Research (IEK-6) Nuclear Waste Management and Reactor Safety, Forschungszentrum Jülich, Germany, e-mail: k.rozov@fz-juelich.de
Hilde Curtius, Dirk Bosbach: Institute of Energy and Climate Research (IEK-6) Nuclear Waste Management and Reactor Safety, Forschungszentrum Jülich, Germany

Keywords: Solid solution, isostructural substitution, layered double hydroxides, thermodynamic modeling, anionic clays, hydrotalcites.

DOI 10.1515/ract-2014-2326
Received August 14, 2014; accepted November 13, 2014

1 Introduction

The disposal of radioactive waste materials at geological conditions requires the development of physically and chemically stable materials which will prevent the migration of various (i.e., cationic and anionic) radioactive compounds and their decay products from deep geological environments to the biosphere. Layered double hydroxides (LDHs) or hydrotalcite-like solids are of interest of these studies due to their unique properties to immobilize very wide range of cations (like, Li^+, Ba^{2+}, Mg^{2+}, Fe^{2+}, Ni^{2+}, Co^{2+}, Eu^{3+}, Fe^{3+}, Cr^{3+}, Ga^{3+}, Sc^{3+}, Zr^{4+}, etc.) [1–9] and especially due to their anion-exchange properties (substitution of I^-, Br^-, Cl^-, OH^-, CO_3^{2-}, SO_4^{2-}, $Fe(CN)_6^{4-}$, carboxylates, sulfonates or dicarboxylates $C_nH_{2n}(CO_2^-)_2$, etc.) [10–17]. The anion-exchange properties of LDHs are directly attributed with their structure consisting on positive charged octahedral brucite-like layers $[M^{II}_{(1-x)}M^{III}_{(x)}(OH)_2]^{x+}$. The charge deficit of the octahedral layers is compensated by intercalated interlayer anions which are accompanied by molecules of water $[A^y_{x/y} \cdot nH_2O]$. Therefore, LDHs can be considered as potential buffer materials for retention of mobile and hazardous anionic radionuclides (like, ^{14}C, ^{129}I, ^{36}Cl, ^{79}Se, TcO_4^-, etc.) [18]. At the present time the application of LDHs as anion-binding material is problematic task due to their chemical complexity when LDHs have to be considered as complex multicomponent solid solutions which thermodynamic, mixing and solubility properties are hardly achievable. Consequently, there is a problem to apply LDHs for geochemical modeling (partially at conditions of nuclear waste repositories). The present study is focused on the synthesis, characterization of a particular case of big LDH family, namely, chloride-bearing hydro-

talcite (Htlc) $Mg_3Al(OH)_8Cl \cdot nH_2O$ where the isostructural incorporation of Zr(IV) is expected. The selection of this system was based on the knowledge that similar Fe-containing LDHs were already identified as characteristic secondary phases when research nuclear fuel elements were in the contact with salt brine solutions under repository relevant conditions [5]. To investigate the incorporation of tetravalent cations into the LDH structure is interesting task because there is no clarity concerning incorporation of tetravalent metals in LDHs. Some of studies reported the possibility of synthesizing LDHs containing M(IV) ions [5, 19–24]. Another authors based on results of X-ray absorption spectroscopy (XAS) and Mössbauer spectroscopy [25] concluded that the M(IV) cations are segregated from LDH structure and may form amorphous M(IV) oxide-like particles. In our study the main reason to investigate the possibility of Zr-containing LDH formation was the expectation that the incorporation of tetravalent cation has to affect on anion-exchange properties of LDHs due to the change of positive charge in brucite-like layers. Moreover, Zr(IV) can be considered as analogue of 4-valent actinides (i.e., U^{4+} and Th^{4+}) and to investigate the behavior of zirconium is important task from point of view of geochemistry of nuclear waste repositories. Finally, Zr(IV) is an important constituent of nuclear waste repositories because it presented in cladding elements of nuclear fuel. Using various experimental techniques (X-ray powder diffraction, Raman spectroscopic measurements, scanning electron microscopy, energy dispersive X-ray spectroscopy), the primary objective of this work was to explore the isostructural incorporation of Zr into the hydrotalcite structure (i.e., to proof the presence of solid solutions). The next objectives were: 1) to quantify stability properties (i.e., standard Gibbs free energies of formation) of Zr-containing LDHs with the help of thermodynamic modeling [26, 27]; 2) to develop the provisional scheme of Zr-substitution in the hydrotalcite structure.

2 Experimental

2.1 LDH synthesis

Samples of LDH solids with varying zirconium $x\mathrm{Zr}_{\mathrm{solid}} = \mathrm{Zr}/(\mathrm{Zr}+\mathrm{Al})$ mole fractions were synthesized by a co-precipitation method at $T = 25 \pm 2\,^{\circ}\mathrm{C}$ and $\mathrm{pH} = 10.00 \pm 0.05$. The synthesis procedure was based on the slow (0.2–0.3 mL/min) addition of 40 mL degassed metal-chloride solution with $\mathrm{Mg}/(\mathrm{Al}+\mathrm{Zr}) = 3.0 \pm 0.1$ and desired $\mathrm{Zr}/(\mathrm{Zr}+\mathrm{Al})$ ratios into the reactor vessel containing 250 mL of boiled MilliQ water under stirring and under argon gas flow. The total concentration of Mg, Al and Zr in metal-chloride solution was 0.8 moles/L. Simultaneously 2 M NaOH solution was added into the reactor by using an automated titrator 736 GP TITRINO in order to maintain $\mathrm{pH} = 10.00 \pm 0.05$ constant. After the addition step, the stirring of suspension was continued for approximately 24 h under the controlled $\mathrm{pH} = 10.00 \pm 0.05$. Then precipitate and supernatant liquid were separated by using 0.22 μm MILLEX® GP filters. The formed solid product was washed three times by boiled degassed MilliQ water and finally dried in a desiccator for 72 h.

2.2 Chemical analyses of solid and liquid phases

The contents of Mg, Al and Zr in the solids and aqueous solutions after syntheses have been determined by ICP-OES method using TJA-IRIS™ instrument. The aqueous solutions after syntheses were analyzed after acidifying with approximately 0.5 mL of 8 M HNO_3. Samples of solid phases were analyzed after dissolving in 2 M HNO_3. Internal standard solutions were prepared from $MgCl_2 \cdot 6H_2O$, $AlCl_3 \cdot 6H_2O$ and $ZrOCl_2 \cdot 8H_2O$ chemicals (Merck®).

2.3 Photometric analyses

Chloride anions in the product liquid phase and in synthesized solids were analyzed photometrically (spectrophotometer CADAS 100). The sample preparation and analysis procedure are described in details in [7].

2.4 Powder X-ray diffraction

The powder X-ray diffraction measurements were applied for structural characterization of synthesized solids. The patterns were recorded using 3003 TT (General Electric®) diffractometer (Bragg–Brentano geometry) at the ambient temperature within a 2θ-range from 5 to 80° with a step size of 0.02° 2θ and a measuring time of 15 s per step. Unit-cell parameters ($a_0 = b_0$ and c_0) of pure Zr-LDH solids have been estimated applying a Bragg-type equation and using relation between indexed d_{hkl} distances and the lattice unit-cell parameters for hexagonal symmetry based on the first 4 reflections: (003), (006), (012), and (015). The scheme of these estimations is described in details previously [7, 28, 29].

2.5 Raman spectroscopy

Raman spectroscopic measurements have been carried out to identify the type of anion in the interlayer space of LDH structure. Raman scattering spectra were acquired using a LabRAM HR Vis® spectrometer equipped with 632.81 nm laser and recorded in wavenumber interval from 200 to 3800 cm^{-1}. The spectra were calibrated using Si standard. The data were manipulated and recorded using LabSpec v.5. software. The band component analysis was carried out using "Fityk" (http://fityk.nieto.pl/) software, and the band fitting and smoothing were done using Gaussian functions.

2.6 Scanning electron microscopy (SEM) and energy dispersive X-ray spectroscopy (EDX)

The low-pressure scanning electron microscopy (SEM) was performed with Quanta 200® microscope in order to investigate the morphology of synthesized crystallites. Examinations were performed at 70 Pa. Analyses of solids (Mg, Al, Zr, O, Cl, C, O) and the information about chemical homogeneity were performed with EDX spectroscopy by using Appolo X Silicon Drift Detector from EDAX™, at a voltage 20 kV.

2.7 Thermodynamic modeling and estimation of Gibbs free energies

The thermodynamic modeling has been performed assuming the thermodynamic equilibrium between precipitates and aqueous solutions after syntheses. This assumption was made based on previous results [29] which demonstrated that the degree of oversaturation in liquid phase after similar co-precipitation experiments is negligible and precipitates and corresponding aqueous solutions are at conditions which close to the equilibrium. The sequence of calculation steps needed for estimating Gibbs free energies of LDH solids was described in details before [7, 28, 29]. Firstly, by applying GEMS-Selektor v.3. code [26, 27] with built in Nagra-PSI thermodynamic database [18] and by using chemical analyses of aqueous solutions, the speciation of dissolved metals, activities and chemical potentials of relevant components (i.e., Mg^{2+}, Al^{3+}, Zr^{4+}, OH^-, Cl^-) have been calculated. Then the statement which says that: "Gibbs free energy of the system at equilibrium is minimum, and chemical potentials of the components are the same at each phase" allowed to calculate the molar Gibbs free energies from chemical potentials and from stoichiometric coefficients in Table 1 according to equation:

$$G_f^\circ(\mathrm{LDH}) = a \cdot \mu(Mg^{2+}) + b \cdot \mu(Al^{3+}) + c \cdot \mu(Zr^{4+}) + d \cdot \mu(OH^-) + e \cdot \mu(Cl^-) \quad (1)$$

where a–e: stoichiometric coefficients; μ-calculated chemical potentials.

3 Results

3.1 Compositions of solids and liquid phases after co-precipitation experiments

Chemical compositions of pure Zr-containing LDHs and aqueous solutions after syntheses are provided in Tables 1 and 2, respectively.

Results of chemical analyses demonstrated that each formula unit of Zr-bearing LDH contains 7.612 ± 0.285 OH^- and 0.613 ± 0.230 Cl^-. In addition we observed that washed solids contained only traces of Na (less than 1 wt %), which means that the stoichiometric coefficient of sodium in solids was less than $Na_{0.001}$. Table 1 reveals clearly that with the increase of the zirconium mole fraction (xZr_{solid}) from 0.086 to 0.488 in synthesized solid the $Mg/(Al + Zr)$ cationic ratios reduces significantly (from 2.768 to 2.005). It is necessary to remind that for all co-precipitation experiments the $Mg/(Al + Zr)$ ratio in initial metal-containing solutions always was fixed constant (3.0 ± 0.1). We observed that chemical compositions of synthesized solids are well described by $[Mg_{3-2x}Al_{1-x}Zr_x]$ – stoichiometry, where x – is the mole fraction of zirconium. The correctness of this statement has been additionally proofed by comparing measured $a_0 = b_0$ unit-cell distances in solids and those theoretical values obtained from regular octahedral brucite-like layers having $[Mg_{3-2x}Al_{1-x}Zr_x]$-stoichiometry (see Section 3.2). Moreover, based on these stoichiometry variations it can be expected that the incorporation of 1 Zr-containing specie in to the pure $Mg_3Al_1(OH)_8Cl_1$ composition results in removal of 2 Mg- and 1 Al-containing species. In details this provisional scheme is described in Section 3.3. As seen in Table 2 measured concentrations of dissolved Mg, Cl and Na are varying on the millimolal level (4.76–51.26, 180–200, 157.69–190.49 mmol/kg, respectively). At the same time concentrations of dissolved Al and Zr are lower than the detection limit of ICP-OES method. Therefore, for further modeling and for determining chemical potentials of Al^{3+} and Zr^{4+} species, the total dissolved molalities of

Table 1: Stoichiometric formulae and estimated standard Gibbs free energies (G_f^o) of formation of Zr-containing LDHs synthesized at $T = 25 \pm 2\,^{\circ}C$ and pH = 10.00 ± 0.05.

Chemical compositions of "water-free" solids	Mole fraction of zirconium in solid phase ($x\mathrm{Zr}_{solid}$)	Mg/(Al + Zr) in solid phase	G_f°, [kJ/mol]
$Mg_{2.768}Al_{0.914}Zr_{0.086}Cl_{0.577}(OH)_{8.045}$	0.086	2.768	−3459.41
$Mg_{2.681}Al_{0.862}Zr_{0.138}Cl_{0.638}(OH)_{7.862}$	0.138	2.681	−3387.37
$Mg_{2.662}Al_{0.814}Zr_{0.186}Cl_{1.026}(OH)_{7.484}$	0.186	2.662	−3384.78
$Mg_{2.410}Al_{0.733}Zr_{0.267}Cl_{0.575}(OH)_{7.512}$	0.267	2.410	−3222.86
$Mg_{2.527}Al_{0.709}Zr_{0.291}Cl_{0.751}(OH)_{7.594}$	0.291	2.527	−3320.76
$Mg_{2.326}Al_{0.635}Zr_{0.365}Cl_{0.381}(OH)_{7.636}$	0.365	2.326	−3193.11
$Mg_{2.005}Al_{0.512}Zr_{0.488}Cl_{0.346}(OH)_{7.152}$	0.488	2.005	−2971.14

Table 2: Compositions of aqueous solutions (pH = 10.00 ± 0.05) after LDHs syntheses at $T = 25 \pm 2\,^{\circ}C$.

Mole fraction of Zr in solids ($x\mathrm{Zr}_{solid}$)	Mg	Cl	Na	Al	Zr
	[mmol/kg]			[μmol/kg]	
0.086	4.76	199.00	184.76	1.14	0.51
0.138	51.26	192.00	190.49	1.14	0.51
0.186	7.01	180.00	169.19	1.10	0.54
0.267	8.60	200.00	174.33	1.14	0.51
0.291	8.27	191.00	177.07	1.14	0.51
0.365	14.95	195.00	169.48	1.10	0.54
0.488	19.40	187.00	157.69	1.10	0.54

these metals were assumed to be on the level 1.10–1.14 and 0.51–0.54 μmol/kg, respectively (i.e., detection limit of ICP-OES for these metals). In conclusion we see that the ionic strength (~0.2 M) of all "syntheses solutions" is generally defined by sodium concentrations and this fact permitted the use Davies model [30] for estimating activities and chemical potentials of relevant dissolved components.

3.2 Characterization of synthesized solids by PXRD, Raman spectroscopy, SEM and EDX techniques

PXRD technique has been used in order to proof that synthesized solids are indeed pure Zr-containing hydrotalcite-like solids and, thereby, to check that Zr is structurally incorporated in the LDHs. Moreover, PXRD approach could be applied to construct the provisional scheme of Zr incorporation into the structure of hydrotalcite-like solids.

We observed that precipitates with the mole fraction of zirconium with $0 \le x\mathrm{Zr}_{solid} \le 0.5$ display only X-ray patterns (Figure 1a) typical for pure hydrotalcite-like solids. The increase of $x\mathrm{Zr}_{solid}$ in pure LDH solids is accompanied with the widening of X-ray reflexes and, therefore, may indicate on: (1) the decrease of crystallite size in solids, or (2) the presence of undetectable amorphous substance (for instance, brucite). The second hypothesis is confirmed by the fact that the background of diffractogramms (Figure 1a) is continuously climbing with the growth of $x\mathrm{Zr}_{solid}$. In synthesized phases with $x\mathrm{Zr}_{solid} > 0.5$ we observed additional X-ray reflexes attributed to brucite (see light-gray circles on Figure 1b).

Evaluated unit-cell parameters $a_0 = b_0$ reflex intermetallic distances in octahedral brucite-like layers in the LDH structure and shown as a function zirconium content ($x\mathrm{Zr}_{solid}$) (Figure 2a) and as a function of Mg/(Al + Zr) cationic ratio (Figure 2b). As seen on Figure 2, $a_0 = b_0$ unit-cell distances are generally correlating with these compositional changes. Moreover, the theoretical values of $a_0 = b_0$ unit-cell parameters were calculated based on the regular brucite-like layers having $[Mg_{3-2x}Al_{1-x}Zr_x]$-stoichiometry (where ionic radii of cations in octahedral coordination are $r_{Mg^{2+}} = 0.720$ Å, $r_{A^{3+}} = 0.535$ Å, $r_{Zr^{4+}} = 0.720$ Å) [31]. Figure 2 is demonstrating that theoretical dependences of $a_0 = b_0$ (solid curves) are generally consistent with experimental values. Therefore, this fact can indicate that $[Mg_{3-2x}Al_{1-x}Zr_x]$-stoichiometry may describe the variety of chemical compositions of precipitates. Moreover, this chemical variability is pointing out on ont the situation when the incorporation of 1 Zr-specie into the hydrotalcite $Mg_3Al_1(OH)_8Cl_1$ structure replaces 2 Mg- and 1 Al-containing species. Nevertheless, the structural position of Zr in LDH solids is still questionable because of the big scatter of measured $a_0 = b_0$ values. The clarifying of the structural position of Zr in the LDH is complicated by the presence in Zr-bearing precipitates of unidentified amorphous phase.

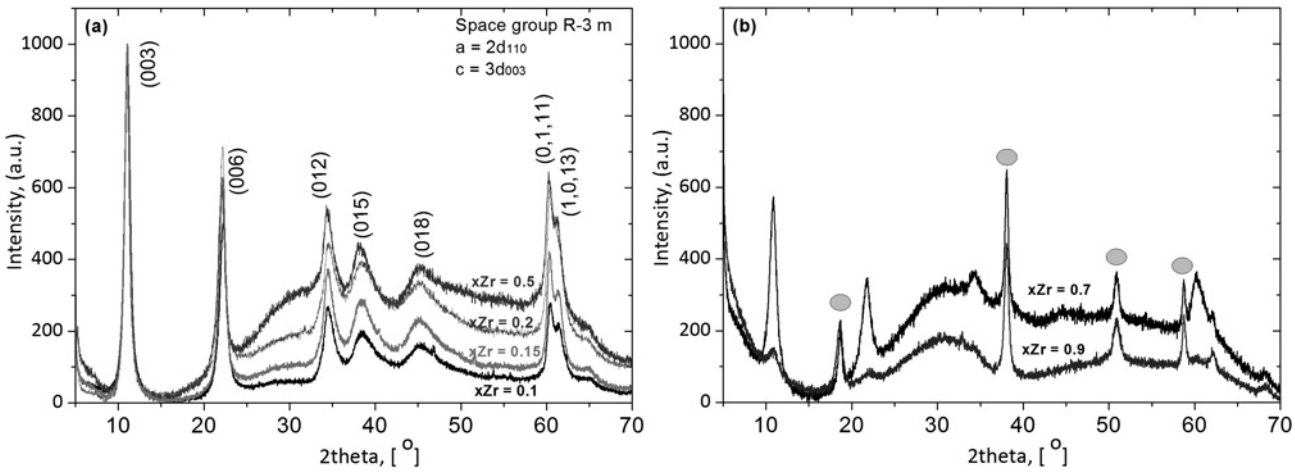

Fig. 1: X-ray diffractograms of Zr-containing LDHs: (a) with $xZr_{solid} \leq 0.5$; and (b) with $xZr_{solid} > 0.5$ (light-gray circles correspond to patterns attributed to brucite).

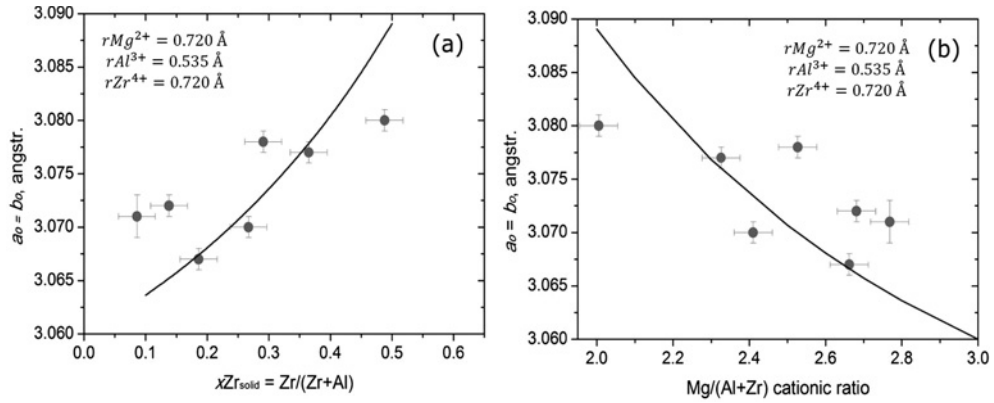

Fig. 2: Unit-cell distances $a_o = b_o$ as a function of $Zr/(Al + Mg)$ the zirconium mole fraction (a) and as a function of $Mg/(Al + Zr)$ cationic ratio (b) in synthesized LDHs. Solid curves represent theoretical estimates based on the regular octahedral brucite-like layers having $[Mg_{3-2x}Al_{1-x}Zr_x]$ – stoichiometry.

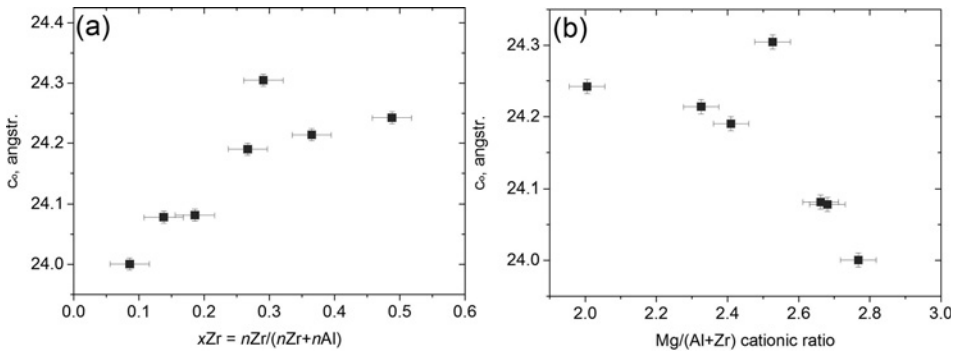

Fig. 3: Unit-cell parameter c_o as a function of $Zr/(Al + Mg)$ the zirconium mole fraction (a) and as a function of $Mg/(Al + Zr)$ cationic ratio (b) in synthesized LDHs.

Unit-cell parameters c_0 of pure Zr-LDH solids as a function of xZr_{solid} mole fraction and as a function of $Mg/(Al + Zr)$ cationic ratio are shown on Figure 3a and b, respectively.

As seen on Figure 3a and b the increase of unit-cell parameter c_0 is related with the growth of Zr-content (and corresponding decrease of $Mg/(Al + Zr)$ ratio) in synthesized solids. At first sight this observation is in the contra-

diction with the solid stoichiometry variations presented in Table 1. The reason is that unit-cell parameter c_0 reflexes mainly changes in the size of the interlayer space of the LDH structure. Therefore, the unit-cell parameter c_0 has to be a very sensitive to compositional changes of the interlayer (content of water, hydroxyl groups, chloride ions). From Table 1 it is clearly seen that there is the decrease of OH^-- and Cl^--contents in LDHs with the growth of $x\mathrm{Zr}_{\mathrm{solid}}$ values. Consequently, it is expected that c_0-value should decrease with the growth of Zr-content. The opposite observation should indicate that: (1) amount of structural water-molecules can increase with growth of Zr-content or (2) there is a substitution of Zr-species in the interlayer space of LDH structure. The first explanation is doubtful because we demonstrated that in all solids the water-content is approximately constant (2.33–2.50 molecules). Therefore, it is necessary to consider the hypothesis which implies the possibility of partial Zr-substitution into the interlayer space. The structural position of Zr-atoms in LDHs may be elaborated by applying different approaches. Particularly, the Rietveld structural refinements would help to specify the structural rearrangements of Zr in the LDH structure. However, at the present study these refinements were not performed because of the poor crystallinity of synthesized precipitates. Consequently, we were focused on other available approaches to identify the coordination environment of Zr in the LDH structure (i.e., thermodynamic modeling with GEMS-Selektor v.3. code) (see Section 3.3).

Raman spectroscopy has been used as suitable method for identifying the nature of the interlayer anions. Raman bands (around 467, 546, 1060, 3450 and 3700 cm^{-1}) which are typical for hydrotalcite-like solids [32] have been observed. Typical Raman spectra of synthesized LDHs with $x\mathrm{Zr}_{\mathrm{solid}} \approx 0.10$ are displayed on Figure 4. The band detected around 467 cm^{-1} is unique for hydrotalcite-like solids and assigned to the Me-O-Me linkage bonding [33]. The band around 546 cm^{-1} is presented in all Raman spectra of synthesized Zr-containing LDHs and according to [32] originates from the interlayer carbonate-water unit, where two hydrogen atoms of H_2O molecule are interacting with two oxygen atoms of carbonate-anion, strongly indicating the presence of carbonate in the system. The presence of carbonate in precipitates is explained by a very significant affinity of this anion to LDH phases. Carbonate can be contaminated during the synthesis procedure

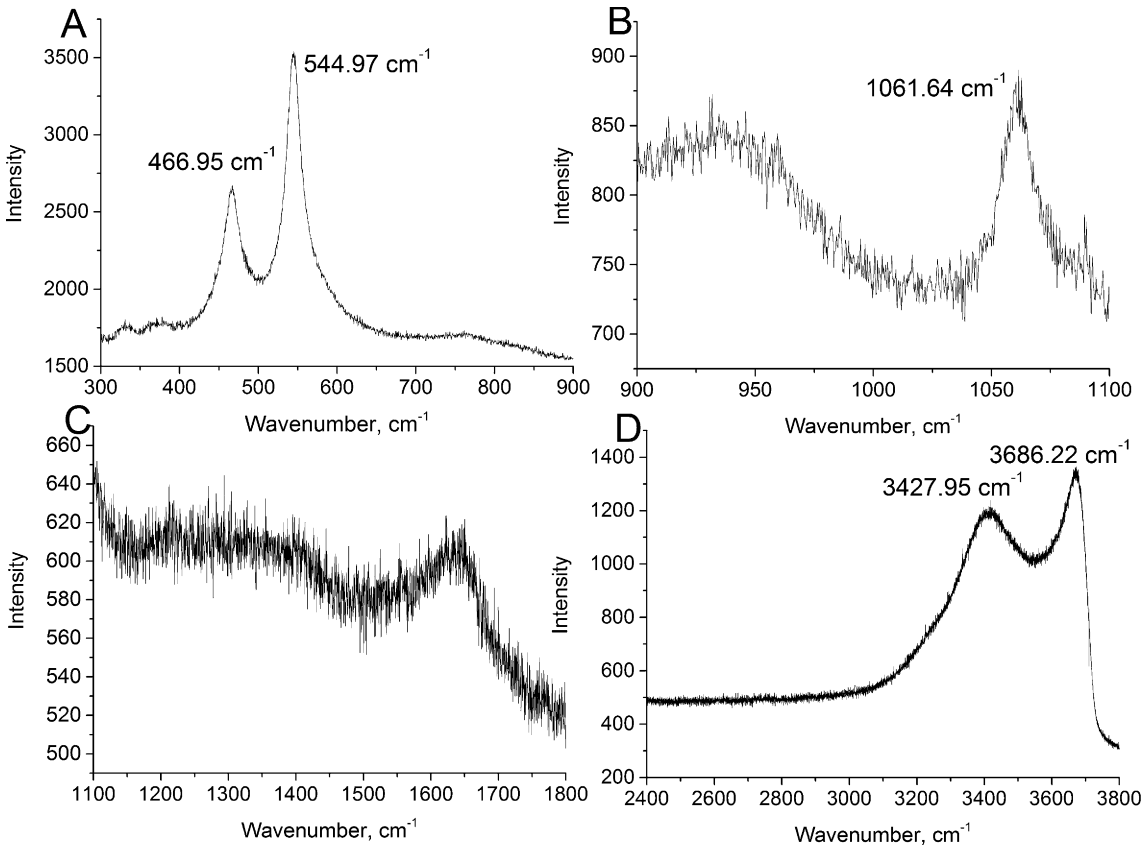

Fig. 4: Raman spectra of Zr-containing LDH with $x\mathrm{Zr}_{\mathrm{solid}} \approx 0.1$. A more detailed description of individual spectra is given in the text.

or/and during the preparation of samples for Raman measurements. The band around 1060 cm^{-1} is also confirming the presence of CO_3^{2-} and corresponds to interlayer carbonate anions associated with $Me(OH)_6$ octahedral units in the brucite-like layers [32]. In the whole range of Zr-content in synthesized hydrotalcite-like solids the position of this peak remains almost constant indicating no change in symmetry of carbonate anions. The large bands around 3450 cm^{-1} and 3700 cm^{-1} represent OH-stretching vibrations from MeOH-groups as well as stretching vibrations of interlayer water molecules. Results of band component analyses demonstrated that the peak positions and intensities of all Raman bands are not correlating with the Zr-content in precipitates.

Scanning electron microscopy demonstrated that the majority of synthesized solids were similar to typical LDHs "sand rose" aggregates. Energy dispersive X-ray analyses shown that in synthesized solids with $x\mathrm{Zr}_{solid}$ from 0 to 0.5 the distribution of Mg, Al, Zr, C, O and Cl components is generally homogeneous and obtained stoichiometric coefficients of precipitates are in good agreement with results of ICP-OES analyses. The chemical homogeneity of samples has been proved by numerous replications (up to 10) of EDX measurements on various regions of LDH grains.

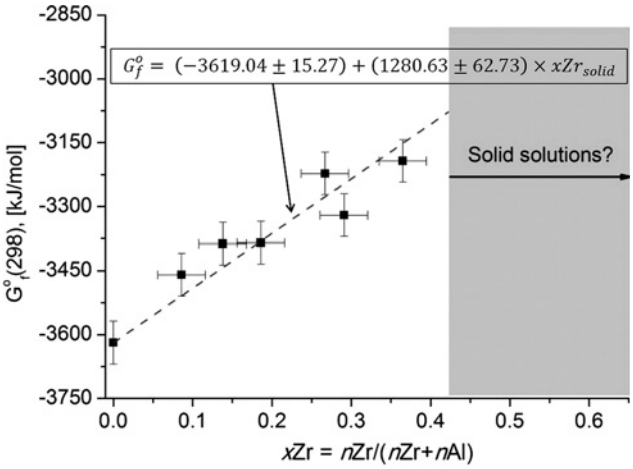

Fig. 5: Standard Gibbs free energies of "water-free" solids calculated as a function of the mole fraction of zirconium.

3.3 Estimation of the standard Gibbs energies and thermodynamic properties of synthesized Zr-containing LDHs

Thermodynamic properties of synthesized Zr-containing LDH solids have been estimated according to the scheme described in Section 2.7 and assuming the thermodynamic equilibrium between precipitates and aqueous solutions after synthesis experiments. This assumption was based on previous results [29] which clearly shown that the degree of oversaturation in liquids after co-precipitation experiments was negligible and, therefore, precipitated solids and corresponding aqueous solutions were at conditions close to thermodynamic equilibrium. On Figure 5 the calculated values of standard molar Gibbs free energies of solids are shown as a function of Zr-content (i.e., Zr/(Zr + Al) ratios in solids). Moreover, from this figure it is clear that the addition of only 0.1 units of zirconium into the hydrotalcite structure increases the value of standard Gibbs free energy significantly (approximately 100 kJ/mol). The reason of this increase has to be related with structural modifications originating from the Zr-incorporation into pure Mg-Al-LDH composition. The obvious explanation of this major effect of zirconium may be that Zr occupies the interlayer space in hydrotalcite structure and, therefore, significantly disturbing the structural stability of LDHs. As mentioned in Section 3.2, in the present study we were not able to check this hypothesis by applying analytical and spectroscopic methods. Therefore, only theoretical thermodynamic considerations have been used. On the first step, the compositions of aqueous solutions after syntheses have been modeled by using GEM-Selektor code package as described before and predominant aqueous complexes of Mg, Al and Zr were determined. Results of the modeling shown that at conditions of syntheses (pH = 10.00 ± 0.05, $T = 25-2\ ^{\circ}C$) the dissolved metals have to be mainly presented as Mg^{2+}, $Al(OH)_4^-$ and $Zr(OH)_5^-$ aqueous species. Thus, from this result we can suppose that Zr could play a role of "anionic" $Zr(OH)_5^-$ constituent and it can be incorporated (at least partially) into the interlayer between brucite-like layers. The possible reaction of such incorporation of Zr into the pure Mg-Al-LDH is written as:

$$Mg_3Al(OH)_8Cl_{1(s)} + Zr(OH)_{5(aq)}^- = Mg_1Zr_1(OH)_5Cl_{1(s)} + Al(OH)_{4(aq)}^- + 2Mg_{(aq)}^{2+} + 4OH_{(aq)}^-, \quad (2)$$

where $Mg_1Zr_1(OH)_5Cl_1$ composition is corresponding to the "hypothetical" end-member according to discovered $[Mg_{3-2x}Al_{1-x}Zr_x]$-stoichiometry ($x\mathrm{Zr}_{solid} = 1$). Thermodynamically the Reaction 2 seems to be reasonable: assuming the equilibrium (i.e., $\Delta_r G = 0$) and by using known values (see Table 3) of the molar Gibbs free energies of $Mg_3Al_1(OH)_8Cl_1$, $Zr(OH)_5^-$, $Al(OH)_4^-$, Mg^{2+}, OH^-, the molar Gibbs free energy of formation of $Mg_1Zr_1(OH)_5Cl_1$

Table 3: Standard molar Gibbs free energies used in thermodynamic calculations.

Substance/Complex	G_f^o, [kJ/mol]	Reference
$Mg_3Al_1(OH)_8Cl_{1(s)}$	−3619.04 ± 15.27	(1)
$Zr(OH)_{5(aq)}^-$	−1177.82	(2)
$Al(OH)_{4(aq)}^-$	−827.48	(2)
$Mg_{(aq)}^{2+}$	−453.99	(2)
$OH_{(aq)}^-$	−157.27	(2)

(1) – Rozov et al., 2013; (2) – Hummel et al., 2002.

stoichiometry composition will correspond to:

$$G_f^\circ[Mg_1Zr_1(OH)_5Cl_1]_{(s)} = G_f^\circ[Mg_3Al_1(OH)_8Cl]_{(s)} + G_f^\circ[Zr(OH)_5^-]_{(aq)} - G_f^\circ[Al(OH)_4^-]_{(aq)} - 2G_f^\circ[Mg^{2+}]_{(aq)} - 4G_f^\circ[OH^-]_{(aq)} = -2432.33 \pm 15.27\ \text{kJ/mol} \quad (3)$$

This value (−2432.33 ± 15.27 kJ/mol) is in a good agreement with the number (−2338.41 ±64.56 kJ/mol) obtained from the linear approximation $G_f^0 = (-3619.04 \pm 15.72) + (1280.63 \pm 62.73) \times x\text{Zr}_{\text{solid}}$ shown on Figure 5. This fact may support additionally the proposed substitution mechanism.

4 Conclusions

The aim of the present work was to investigate the possibility of the isostructural substitution of tetravalent cations (particularly, zirconium) into the hydrotalcite-like solids by using results of co-precipitation experiments carried out at ambient conditions ($T = 25 \pm 2\ ^\circ\text{C}$, $P = 1$ bar), applying various characterization techniques and considering results of thermodynamic modeling. The scheme (see Figure 6) has been constructed in order to reflect clearly the sequence of experimental observations and corresponding interpretations. This diagram helped to formulate the provisional scheme Zr incorporation into the hydrotalcite structure.

Firstly, results of PXRD technique demonstrated that hydrotalcite-like solids with variable Zr-content ($0 < x\text{Zr}_{\text{solid}} \leq 0.5$) have been successfully synthesized. Nevertheless, in precipitates with $x\text{Zr}_{\text{solid}} > 0.5$ the additional X-ray diffraction reflexes attributed to brucite were observed.

Results of chemical analyses demonstrated that the Mg/(Al + Zr) cationic ratios in pure Zr-bearing hydrotalcites are significantly reducing (from 3 to 2) with the increase of Zr-mole fraction (Zr/(Zr + Al)) in spite of the constant Mg/(Al + Zr) = 3.0 ± 0.1 ratio in initial metal-containing solutions used for experiments. These stoichiometric variations allowed summarizing the composition of cationic part of brucite-like layers as $[Mg_{3-2x}Al_{1-x}Zr_x]$. Considering $x = 0$ and $x = 1$ for this stoichiometry it is obviously to conclude that the incorporation of 1 Zr-containing specie results in the removal of 2 Mg- and 1 Al-containing species from pure Mg-Al hydrotalcite end-member. Nevertheless, from this fact it is not possible to specify the structural position of incorporated Zr. Therefore, we used results of PXRD technique and observed that $a_0 = b_0$ unit-cell parameters of pure Zr-containing LDHs are related with those compositional variations

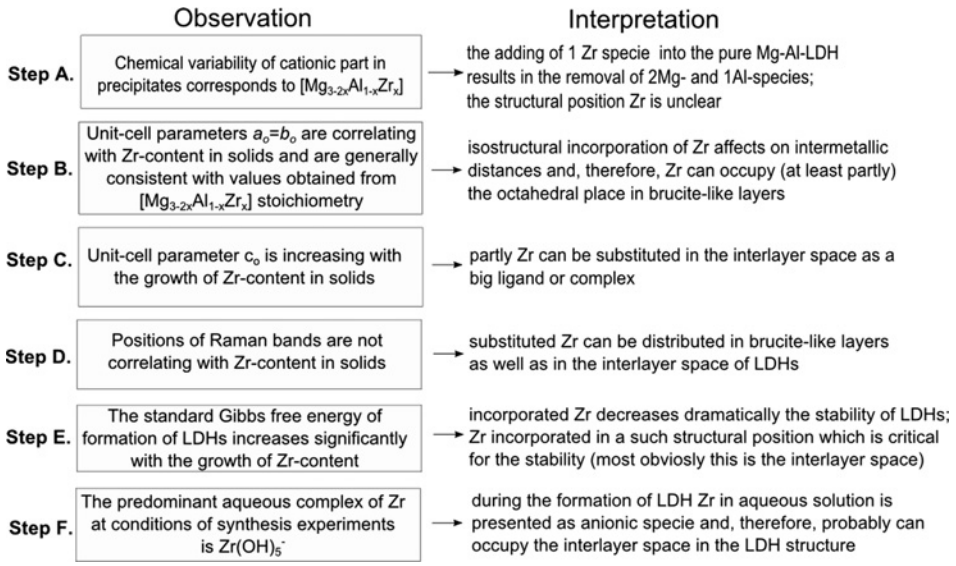

Fig. 6: Logic chart representing the sequence of experimental observations and corresponding interpretations.

($x\mathrm{Zr}_{solid}$ and Mg/(Al + Zr) ratios). Measured $a_0 = b_0$ distances were compared with values obtained from theoretical $[Mg_{3-2x}Al_{1-x}Zr_x]$-stoichiometry which corresponds to regular octahedral layers and the general coincidence between them has been found. This fact can indicate that Zr incorporation affects on intermetallic distances in brucite-like layers and, thus, Zr can be substituted in the octahedral positions of brucite-like layers. On the other hand, unit-cell parameter c_0 represents the interlayer distance between brucite-like layers is also correlating with Zr content in LDHs. Therefore, it is possible to suppose that some part of Zr can be substituted in the interlayer space.

Results of Raman spectroscopic measurements demonstrated that synthesized LDHs have a very strong affinity to carbonate-anions: in all precipitates the bands around 546 cm^{-1} (attributed to the interlayer carbonate and water molecules), 1060 cm^{-1} (interaction of carbonate with $Me(OH)_6$ octahedral units) were detected. Raman bands typical for hydrotalcite-like solids have been detected in regions aroung 467 cm^{-1} (assigned to the Me-O-Me linkage bonding), 3450 and 3700 cm^{-1} (OH-stretching vibrations from MeOH-groups of brucite-like layers as well as stretching vibrations of interlayer water molecules). The dependence of positions of all Raman bands on Zr-content was not observed indicating implicitly that Zr-species can occupy simultaneously structural positions in brucite-like layers and in interlayers.

In order to corroborate the hypothesis that Zr is partly incorporated in the interlayer space of LDH structure, the thermodynamic modeling with GEMS-Selektor code v.3. has been applied. The standard Gibbs free energies of formation for pure precipitates have been estimated assuming the thermodynamic equilibrium between solids and supernatant solutions after experiments. The observed correlation between the standard Gibbs free energies and Zr-content in these solids demonstrates that the addition of small traces of zirconium decreases significantly the stability of synthesized solids. For instance, the addition of only 0.1 molar unit of Zr-mole fraction increases the standard Gibbs free energy by approximately 100 kJ/moles. Furthermore, results of modeling demonstrated that at conditions of co-precipitation experiments Mg, Al and Zr in aqueous solution are presented as Mg^{2+}, $Al(OH)_4^-$ and $Zr(OH)_5^-$ complexes. Therefore, it is likely that zirconium is substituted into the hydrotalcite structure as negative-charged "anionic" compound and, consequently, it can be localized in the interlayer space. In such case the significant decrease of hydrotalcite stability with addition of zirconium is reasonably explainable. The reaction of Zr-substitution will be written as: $Mg_3Al(OH)_8Cl_{1(s)} + Zr(OH)_{5(aq)}^- = Mg_1Zr_1(OH)_5Cl_{1(s)} + Al(OH)_{4(aq)}^- + 2\,Mg_{(aq)}^{2+} + 4\,OH_{(aq)}^-$. The value of the standard Gibbs free energy of formation for $Mg_1Zr_1(OH)_5Cl_1$-composition has been obtained from this reaction and is in the excellent agreement with estimate calculated from the linear approximation presented on Figure 5.

Finally, the statement which is formulating the scheme of Zr-incorporation into the hydrotalcite structure is: "zirconium can be structurally incorporated into the LDH. At that, zirconium can occupy two structural sites in hydrotalcite-like solids: in octahedral brucite-like layers and in the interlayer space as $Zr(OH)_5^-$ ligands. This situation leads to very significant decrease of stability of LDHs even if very small Zr-content in the LDH is included. The adding of higher amounts of Zr into the hydrotalcite system ($Zr/(Zr + Al) \geq 0.5$) finally prevents the formation of sequences of brucite-like layers. Therefore, the fine-crystalline brucite is detected by PXRD method as secondary phase in precipitates with $x\mathrm{Zr}_{solid} \geq 0.5$". Further spectroscopic investigations (for instance, EXAFS analyses) will be applied to specify the coordination environment of zirconium in the LDH structure.

Acknowledgement: We thank Dr. Hartmut Schlenz, Jakob Dellen – for their help with PXRD and Raman spectroscopy; Dr. Andrey Bukaemskiy, Dr. Martina Klinkenberg – for their support with SEM/EDX measurements; Zaina Paparigas, Katharina Dahmen, Gabriel Kaiser – for support in the lab. The study has been funded in part by Bundesministerium für Bildung und Forschung through grant 02NUK019C.

References

1. Aramendia, M. A., Borau, V., Jimenez, U., Marinas, J. M., Ruiz, J. R., Urbano, F. J.: Comparative study of Mg/M(III) (M = Al, Ga, In) layered double hydroxides obtained by coprecipitation and the sol-gel method. Journal of Solid State Chemistry **168**, 156–161 (2002).
2. Boclair, J. W., Braterman, P. S., Jiang, J. P., Lou, S. W., Yarberry, F.: Layered double hydroxide stability. 2. Formation of Cr(III)-containing layered double hydroxides directly from solution. Chemistry of Materials **11**, 303–307 (1999).
3. Carteret, C., Gregoire, B., Ruby, C.: Tunable composition of Ni-II-Al-III and Ni-II-Fe-III layered hydroxides within a wide range of layer charge. Solid State Science **13**, 146–150. (2011)
4. Curtius, H., Paparigas, Z., Kaiser, G.: Sorption of selenium on Mg-Al and Mg-Al-Eu layered double hydroxides. Radiochimica Acta **96**, 651–655 (2008).
5. Curtius, H., Ufer, K., Dardenne, K.: Preparation and characterization of Zr-IV-containing Mg-Al-Cl layered double hydroxide. Radiochimica Acta **97**, 423–428 (2009).

6. Rousselot, I., Taviot-Gueho, C., Leroux, F., Leone, P., Palvadeau, P., Besse, J. P.: Insights on the structural chemistry of hydrocalumite and hydrotalcite-like materials: Investigation of the series $Ca_2M^{3+}(OH)_6Cl \cdot 2H_2O$ (M^{3+}: Al^{3+}, Ga^{3+}, Fe^{3+}, and Sc^{3+}) by X-ray powder diffraction. Journal of Solid State Chemistry **167**, 137–144 (2002).
7. Rozov, K., Curtius, H., Neumann, A., Bosbach, D.: Synthesis, characterization and stability properties of Cl-bearing hydrotalcite-pyroaurite solids. Radiochimica Acta **101**, 101–109 (2013).
8. Ulibarri, M. A., Cornejo, J., Hernandez, M. J.: Effects of hydrothermal treatment on textural properties of $Al_2Li(OH)_6CO_3 \cdot nH_2O$. Journal of Material Science **22**, 1168–1172 (1987).
9. Wang, J. D., Serrette, G., Tian, Y., Clearfield, A.: Synthetic and catalytic studies of inorganically pillared and organically pillared layered double hydroxides. Applied Clay Science **10**, 103–115 (1995).
10. Allada, R. K., Navrotsky, A., Boerio-Goates, J.: Thermochemistry of hydrotalcite-like phases in the MgO-Al_2O_3-CoO_2-H_2O system: a determination of enthalpy, entropy and free energy. American Mineralogist **90**, 329–335 (2005).
11. Brindley, G. W., Kikkawa, S.: Thermal-Behavior of Hydrotalcite and of Anion-Exchanged Forms of Hydrotalcite. Clays and Clay Minerals **28**, 87–91 (1980).
12. Carlino, S.: The intercalation of carboxylic acids into layered double hydroxides: A critical evaluation and review of the different methods. Solid State Ionics **98**, 73–84 (1997).
13. Carrado, K. A., Kostapapas, A., Suib, S. L.: Layered Double Hydroxides (LDHs), Solid State Ionics **26**, 77–86 (1988).
14. Chibwe, K., Jones, W.: Intercalation of Organic and Inorganic Anions into Layered Double Hydroxides, Journal of Chemical Society 926–927 (1989).
15. Chisem, I. C., Jones, W.: Ion-Exchange Properties of Lithium Aluminum Layered Double Hydroxides. Journal of Materials Chemistry **4**, 1737–1744 (1994).
16. Miyata, S., Kumura, T.: Synthesis of New Hydrotalcite-Like Compounds and Their Physicochemical Properties. Chemistry Letters 843–848 (1973).
17. Newman, S. P., Jones, W.: Synthesis, characterization and applications of layered double hydroxides containing organic guests. New Journal of Chemistry **22**, 105–115 (1998).
18. Hummel, W.: Nagra/PSI Chemical Thermodynamic Data Base 01/01. Universal-Publishers, 2002.
19. Das, N., Samal, A.: Synthesis, characterisation and rehydration behaviour of titanium(IV) containing hydrotalcite like compounds. Microporous and Mesoporous Materials **72**, 219–225 (2004).
20. Tichit, D., Das, N., Coq, B., Durand, R.: Preparation of Zr-containing layered double hydroxides and characterization of the acido-basic properties of their mixed oxides. Chemistry of Materials **14**, 1530–1538 (2002).
21. Velu, S., Ramaswamy, V., Ramani, A., Chanda, B. M., Sivasanker, S.: New hydrotalcite-like anionic clays containing Zr^{4+} in the layers. Chemical Communications 2107–2108 (1997).
22. Velu, S., Sabde, D. P., Shah, N., Sivasanker, S.: New hydrotalcite-like anionic clays containing Zr^{4+} in the layers: Synthesis and physicochemical properties. Chemistry of Materials **10**, 3451–3458 (1998).
23. Velu, S., Suzuki, K., Kapoor, M. P., Tomura, S., Ohashi, F., Osaki T.: Effect of Sn incorporation on the thermal transformation and reducibility of $M(II)Al$-layered double hydroxides $M(II) = Ni$ or Co. Chemistry of Materials **12**, 719–730 (2000).
24. Velu, S., Suzuki, K., Okazaki, M., Osaki, T., Tomura, S., Ohashi, F.: Synthesis of new Sn-incorporated layered double hydroxides and their thermal evolution to mixed oxides. Chemistry of Materials **11**, 2163–2172 (1999).
25. Intissar, M., Jumas, J. C., Besse, J. P., Leroux, F.: Reinvestigation of the layered double hydroxide containing tetravalent cations: Unambiguous response provided by XAS and Mossbauer spectroscopies. Chemistry of Materials **15**, 4625–4632 (2003).
26. Kulik, D. A., Wagner, T., Dmytrieva, S. V., Kosakowski, G., Hingerl, F. F., Chudnenko, K. V., Berner, U. R.: GEM-Selektor geochemical modeling package: revised algorithm and GEMS3K numerical kernel for coupled simulation codes. Computational Geosciences **17**, 1–24 (2013).
27. Wagner, T., Kulik, D. A., Hingerl, F. F., Dmytrievava, S. V.: GEM-Selektor geochemical modeling package: TSolMod library and data interface for multicomponent phase models. Canadian Mineralogist **50**, 1173–1195 (2012).
28. Rozov K., Berner U., Taviot-Gueho C., Leroux F., Renaudin G., Kulik D., Diamond L. W.: Synthesis and chracterization of the LDH hydrotalcite-pyroaurite solid solution series. Cement and Concrete Research **40**, 1248–1254 (2010).
29. Rozov, K. B., Berner, U., Kulik, D. A., Diamond, L. W.: Solubility and thermodynamic properties of carbonate-bearing hydrotalcite-pyroaurite solid solutions with a 3:1 $Mg/(Al + Fe)$ mole ratio. Clays and Clay Minerals **59**, 215–232 (2011).
30. Davies, C. W.: Ion association, Butterworths, Washington, 1962.
31. Shannon, R.: Revised effective ionic radii and systematic studies of interatomic distances in halides and chalcogenides. Acta Crystallographica Section A **32**, 751–767 (1976).
32. Frost, R. L., Reddy, B. J.: Thermo-Raman spectroscopic study of the natural layered double hydroxide manasseite. Spectrochimica Acta Part A-Molecular and Biomolecular Spectroscopy **65**, 553–559 (2006).
33. Palmer, S. J., Frost, R. L.: The Effect of Synthesis Temperature on the Formation of Hydrotalcites in Bayer Liquor: A Vibrational Spectroscopic Analysis. Applied Spectroscopy **63**, 748–752 (2009).